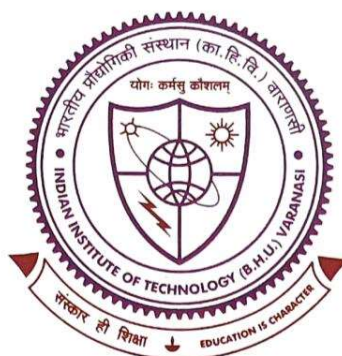


**TUNING OF REDOX ENERGIES BY SYNERGISTIC
INTERACTION OF DIFFERENT TRANSITION METAL IONS
FOR THE DEVELOPMENT OF HIGH-PERFORMANCE
HYBRID SUPERCAPACITORS**



Thesis submitted in partial fulfillment for the
award of degree

Doctor of Philosophy

By

Abhay Narayan Singh

SCHOOL OF MATERIALS SCIENCE AND TECHNOLOGY
INDIAN INSTITUTE OF TECHNOLOGY
(BANARAS HINDU UNIVERSITY)
VARANASI- 221005, INDIA

Roll No. 17111001

Year 2023


Dedicated to my Beloved Family

CERTIFICATE

It is certified that the work contained in the thesis titled “**Tuning of redox energies by synergistic interaction of different transition metal ions for the development of high-performance Hybrid supercapacitors**” by “*Abhay Narayan Singh*” has been carried out under my supervision and that this work has not been submitted elsewhere for a degree.

It is further certified that the student has fulfilled all the requirements of Comprehensive, Candidacy and SOTA for the award of Ph.D. degree.


Dr. (Mrs.) Chandana Rath
Supervisor
Professor/आचार्य
School of Materials Science & Technology/पदार्थ विज्ञान एवं प्रौद्योगिकी स्कूल
Indian Institute of Technology/भारतीय प्रौद्योगिकी संस्थान
(Banaras Hindu University), Varanasi/काशी हिन्दू विश्वविद्यालय, वाराणसी
Indian Institute of Technology (BHU),
Varanasi – 2211005, (U.P.), India


Dr. Preetam Singh
Associate Professor/सह-आचार्य
Department of Ceramic Engineering/सामग्री प्रौद्योगिकी विभाग
Indian Institute of Technology (BHU)
Varanasi-221005/वाराणसी-221005
Department of Ceramic Engineering
Indian Institute of Technology (BHU),
Varanasi – 2211005, (U.P.), India


Dr. Alkesh Kumar Singh
Coordinator & Professor
School of Materials Science & Technology/पदार्थ विज्ञान एवं प्रौद्योगिकी स्कूल
Indian Institute of Technology/भारतीय प्रौद्योगिकी संस्थान
(Banaras Hindu University), Varanasi/काशी हिन्दू विश्वविद्यालय, वाराणसी
School of Materials Science and Technology
Indian Institute of Technology (BHU),
Varanasi – 2211005, (U.P.), India

DECLARATION BY THE CANDIDATE

I, **Abhay Narayan Singh**, certify that the work embodied in this Ph.D. thesis is my own bonafide work carried out by me under the supervision of **Dr. (Mrs.) Chandana Rath** and co-supervision of **Dr. Preetam Singh** for a period from **July 2017** to **July 2023** at the **Indian Institute of Technology (Banaras Hindu University)**, Varanasi, India. The matter embodied in this Ph.D. thesis has not been submitted for the award of any other degree/diploma. I declare that I have faithfully acknowledged and given credits to the research workers wherever their works have been cited in my work in this thesis. I further declare that I have not willfully copied any other's work, paragraphs, text, data, results, *etc.*, reported in journals, books, magazines, reports dissertations, thesis, *etc.*, or available at websites and have not included them in this thesis and have not cited as my own work.

Date.. 28.07.2023

Place: Varanasi

Abhay Narayan Singh
(Abhay Narayan Singh)

CERTIFICATE BY THE SUPERVISOR

This is to certify that the above statement made by the candidate is correct to the best of my knowledge.

Chandana Rath
Dr. (Mrs.) Chandana Rath
Supervisor Professor/आचार्य
School of Materials Science & Technology/पदार्थ विज्ञान एवं प्रौद्योगिकी स्कूल
Indian Institute of Technology/भारतीय प्रौद्योगिकी संस्थान
(Banaras Hindu University), Varanasi/काशी हिन्दू विश्वविद्यालय, वाराणसी


AK Singh
Dr. Akhilesh Kumar Singh
Coordinator/समन्वयक
School of Materials Science & Technology/पदार्थ विज्ञान एवं प्रौद्योगिकी स्कूल
Indian Institute of Technology/भारतीय प्रौद्योगिकी संस्थान
(Banaras Hindu University), Varanasi/काशी हिन्दू विश्वविद्यालय, वाराणसी

Preetam Singh
Dr. Preetam Singh
Associate Professor/सह-आचार्य
Department of Ceramic Engineering
सैरामिक अभियान्त्रिकी विभाग
Indian Institute of Technology (BHU)
भारतीय प्रौद्योगिकी संस्थान (का०हि०वि०वि०)
Varanasi-221005/वाराणसी-221005

COPYRIGHT TRANSFER CERTIFICATE

Title of the Thesis: "Tuning of redox energies by synergistic interaction of different transition metal ions for the development of high-performance Hybrid supercapacitors"

Candidate's Name:



Mr. Abhay Narayan Singh

Copyright Transfer

The undersigned hereby assigns to the Indian Institute of Technology (Banaras Hindu University), Varanasi all rights under copyright that may exist in and for the above thesis submitted for the award of the *Doctor of Philosophy*.

Date: 28-07-2023

Place: Varanasi


(Abhay Narayan Singh)

Note: However, the author may reproduce or authorize others to reproduce materials extracted verbatim from the thesis or derivative of the thesis for the author's personal use provided that the source and the Institute's copyright notice is indicated.

Acknowledgments

At this moment of retrospection, it gives me immense pleasure to acknowledge the persons who have directly or indirectly helped me during the course of my work and stay at IIT (BHU). To express my heartfelt gratitude is not only my moral duty but I consider it an act of pleasure and humility as well.

*First of all, I wish to express my sincere gratitude to my supervisor, **Dr. (Mrs.) Chandana Rath**, for her trust, patience, nice guidance, faithful support and valuable suggestions throughout my Ph.D. work.*

*I am indebted to my thesis co-supervisor, **Dr. Preetam Singh** for his constant monitoring, enthusiastic encouragement, continued guidance, and unconditional support throughout my Ph.D. journey. I always admire his knowledge of the subject, his unconventional thinking, and his enthusiastic nature for research. His ingenious approach to research is a source of inspiration, and this approach is reflected in his simple but clear writing style, which I want to carry forward in my career. I have been fortunate enough to be part of his group. His suggestions and advice will always be beneficial in life, whether it is academic or non-academic. I am very thankful to you sir for being a mentor academically as well as philosophically and wish to continue to seek this mentorship in future life too.*

I would also like to express my sincere thanks to RPEC members Dr. Ashish Kumar Mishra, School of Materials Science & Technology, IIT (BHU) and Dr. Shail Upadhyay, Department of Physics, IIT (BHU), for their stimulating help and criticism which incited me to widen my research from various perspectives. I would like to thank the coordinator of the School of Materials Science and Technology, IIT (BHU) for providing different instrumental facilities.

I would like to extend thanks to Dr. Asha Gupta, Department of Chemistry IIT(BHU) for providing a lab facility during the time of crisis. I also gratefully acknowledge the Ministry of Human Resource and Development; MHRD, India for providing the financial support.

I wish to express eep regards to all the teachers of the School, Prof. D. Pandey, Prof. R. Prakash, Prof. P. Maiti, Dr. B. N. Pal, Dr. C. Upadhyay, Dr. Sanjay Singh, Dr. A. K. Singh, Dr. S. K. Mishra and others for their kind support at all moment during the progress of my research.

With a deep sense of gratitude, I convey my sincere thanks to CIFC, IIT (BHU), Varanasi, (especially to Mr. Shiv Saroj) for help in carrying out characterizations of the synthesized samples. I am also grateful to all office staff of the school and authorities of IIT (BHU), for their kind help during the period of my stay to complete the thesis work.

I also thank my co-authors from whom I have learnt considerably. My sincere gratitude to dear seniors and colleagues: Dr. G.C. Pandey, Dr. Jagdish Kumar G, Dr. Durgesh Kumar, Dr. B. Bharti, Dr. Sandeep Kumar, Dr. Priyanka Tiwaari, Dr. Deepti Gangwar, Mr. Manish Yadav, Mr. Taranga Dehury, Mr. Akhilesh Kumar Yadav, Ms. Sanjna Rajput, Mr. Keshav Kumar, Ms. Aiswarjya Bastia, Mr. Deepankar Das, Ms. Lekshmi S Kumar, Dr. Neeraj Kumar Mishra, Dr. Akanksha Yadav, Dr. Rakesh Mondal, Mr. Neeraj Singh, Mr. Mahatim, Mr. Krishna G. Nigam, Mr. Saurabh. I also want to thank Dr. Asha ma'am research group, Vishal, Vaishali, Shradha for their help and cooperation. I am extremely thankful to my best friend Ms. Neha Berman for her constant support, love, laughter, and motivation to keep me coherent and to make this project possible especially during many rough patches of time.

I would like to thank my friends (Amit, Ajay, Balveer, Shivam, Ved vyas, Priyanka, Pooja, Shanu, Rajpal, Radhey Shyam, M. Alam, Ravi Prakash, Shyam Babu, Gurudev Nirala, Saurabh Pandey, Shashikant, Pragyan, Rahul Singh, Vinod, Rampreet, Ashish Maurya, Dipak Singh, Niraj lal and other junior or senior colleagues) for their friendly support. I wish to express my sincere gratitude to all those who have extended their helping hands in various ways during my tenure at the Indian Institute of Technology (Banaras Hindu University), Varanasi, India. I am also thankful for the negative energies which teach me life lessons and help me to grow.

I would like to express my grateful thanks to my parents (Lt. Brij Mohan Singh and Smt. Malti Devi), my brother, and my sister-in-law (Mr. R. B. Singh & Mrs. Sunita) for their unconditional love, blessings, patience, care, and support in countless ways.

I would like to special thank my sisters (Mrs. Kamala Gandhi, Mrs. Soni Chandel, and Mrs. Priya Soni) for their blessings, love, and constant support. I have also been blessed with my other loving kids (Shalini, Ayush, Jagriti, Samarthya, and Sarthak) for being such a bundle of joy in my life.

Finally, I bow with reverence and gratitude to thank the Almighty Lord KASHI VISHWANATH who has enriched me with such an excellent opportunity and infused the power in my mind to fulfill the work assigned to me.

Date: 28-07-2023

Place: Varanasi

Abhay Narayan Singh
(Abhay Narayan Singh)

List of Figures

Figure 1.1: Different types of non-renewable energy sources	3
Figure 1.2: Different types renewable energy sources	5
Figure 1.3: Worldwide consumption rate of different types energy sources ^{[11][12]}	5
Figure 1.4: Suitability of energy storage technologies to different power and rate of discharge requirements ^[20]	7
Figure 1.5: Different types of grid energy storage technologies ^[21]	8
Figure 1.6: Rangone plot showing energy-power relationship of various EES system ^[28] ..	9
Figure 1.7: Voltaic pile ^[29]	10
Figure 1.8: Schematic presentation of the electrostatic capacitor, electrolytic capacitor, and electrical double layer capacitor ^[38]	12
Figure 1.9: Lead-acid battery ^[41]	14
Figure 1.10: Ni-Cd battery ^[44]	15
Figure 1.11: Schematic diagram of working principle of Zn-air battery ^[54]	16
Figure 1.12: Theoretical energy density, specific energy, and nominal cell voltage of different types of metal-air batteries ^[55]	17
Figure 1.13: Schematic diagram of of Zn-air battery ^[60]	18
Figure 1.14: Basic configuration of a Li-Ion battery ^[62]	19
Figure 1.15: The charge storage mechanism of EDLC ^[73]	21
Figure 1.16: (a) Helmholtz model, (b) Gouy-Chapman model, and (c) Stern Model ^[74] ...	22
Figure 1.17: Schematic representation of Grahame Model ^[75]	23
Figure 1.18: Shows the variation of pseudocapacitance, C_p , and surface coverage, Θ , for ideal Langmuir electrosorption ($g=0$) and Frumkin electrosorption ($g>0$) ^{[74][82]}	24
Figure 1.19: Schematic cyclic voltammograms (a,b,d,e,g,h) and corresponding galvanostatic profiles (c,f,i) of various types of charge storage systems ^[89]	27
Figure 1.20: Li^+ insertion sites in TiO_2 nanoparticles ^[114]	32
Figure 1.21: (A) CVs, (B) b-value determination, (C) derivative of Nb K-edge from in situ XAS, and (D) k^2 -weight FT K-edge from EXAFS at specific potential vs Li/Li^+ ^[116]	33

Figure 1.22: (A) Crystal structure of LaMnO_3 , (B) CVs of $\text{LaMnO}_{2.91}$ in 1M KOH ^[117] , (C) XANES of charged and discharged $\text{PrBaMn}_2\text{O}_{6-\delta}$, and (D) intercalation of O^{2-} in $\text{PrBaMn}_2\text{O}_{6-\delta}$ structure ^[118]	34
Figure 1.23: (a) Standard electrode potential of some common used electrodes, and (b) cell voltage of an aqueous system along with electron energies of active materials ^[120]	35
Figure 1.24: CV and GCD curves of symmetrical EDLC- types of electrodes.	36
Figure 1.25: Schematic illustration of hybrid capacitor ^[126]	37
Figure 1.26: Electrochemical features of $\text{NiO} \parallel \text{Fe}_2\text{O}_3$ device in 6M KOH electrolyte ^[120]	38
Figure 2.1: Schematic diagram of the coprecipitation synthesis of AgFeO_2 nanoparticles	41
Figure 2.2: Schematic growth of the $\text{K}_{0.4}\text{MnO}_2 \cdot x\text{H}_2\text{O}$ crystallites	42
Figure 2.3: Flow chart of the solid-state synthesis of various Sr-doped $\text{Y}_{1-x}\text{Sr}_x\text{MnO}_3$	43
Figure 2.4: Two-step hydrothermal synthesis of different Mn-based layered compounds ($\gamma\text{-MnOOH}$, $\text{LiMnO}_2\text{-Li}_2\text{MnO}_3$, and spinel LiMn_2O_4)	45
Figure 2.5: Different characterization techniques used for the sample analysis	45
Figure 2.6: Schematic diagram illustrating Bragg's law.	47
Figure 2.7: Schematic diagram for the simplified setup of Raman spectroscopy.	50
Figure 2.8: A block diagram of TGA-DSC instrument.	51
Figure 2.9: Schematic working principle of a BET surface area analyser	52
Figure 2.10: Interaction of electrons with sample ^[141]	54
Figure 2.11: Schematic illustration of SEM.	55
Figure 2.12: Block diagram of a commercially available potentiostat (Pine Research) with its equivalent electronic scheme ^[145]	56
Figure 2.13: Three-electrode arrangement used for the electrochemical measurement	57
Figure 2.14: Various types of two-electrode configurations used for the testing of supercapacitor performances ^[146]	58
Figure 2.15: A general electrochemical pathway ^[145]	58
Figure 2.16: (a) Typical cyclic voltammogram depicting the peak position E_P and peak height I_P . (b) CVs for reversible (a), quasi-reversible (b), and irreversible (c) processes. ...	59
Figure 2.17: Represents a typical charge-discharge curve of a supercapacitor.	60
Figure 2.18: (a) Nyquist and (b) Bode plots for both supercapacitors and batteries.	62

Figure 2.19: (A) CVs of nanostructured anatase TiO ₂ films at 0.5 mV/s (B) Charge-storage contribution for different TiO ₂ sizes.	64
Figure 2.20: (A) The potential waveform and current response of aTi ₃ C ₂ T _x MXene electrode in aqueous 3 M H ₂ SO ₄ . (B) Experimental cyclic voltammograms and (C) reconstructed cyclic voltammograms at sweep rates from 2 to 100 mV/s.	65
Figure 3.1: XRD pattern of different electrodes AFO-80, AFO-200, AFO-400, and AFO-550 along with their 2H and 3R JCPDS pattern file.	72
Figure 3.2: Deconvolution of XRD data into two peaks one at 50.52 for the 3R phase (blue solid line) and another at 52.5 for the 2H phase (green solid line) in (a) to (c) whereas in (d) one additional peak at 51.7 correspond to Ag ⁰ (magenta solid line).	73
Figure 3.3: SEM images of the as-obtained samples viz. (a) AFO-80, (b) AFO-400 (fresh) (c) AFO-400 (tested) along with their corresponding EDS images shown in fig. (d), (e), and (f), respectively.	75
Figure 3.4: HRTEM image of 2H (a) and 3R (b) phase of AFO-400 with a lattice spacing of superstructure (inset: inverse FFT of the selected region with their line profile).	76
Figure 3.5: Thermogravimetric analysis (TGA) and differential thermal analysis (DTA) profile of AFO-80 under N ₂ atmosphere.	77
Figure 3.6: Raman (a) and FTIR (b) spectra of different electrodes viz. AFO-80, AFO-200, AFO-400, and AFO-550.	78
Figure 3.7: Represents (a) CV at 10 mV/s scan rate, and (b) GCD at 0.8 A/g current density, AFO-80, AFO-200, AFO-400, and AFO-550.	80
Figure 3.8: (a) CV at different scan rates starting from 1mV/s to 100 mV/s inset show variation in specific capacitance with scan rates, (b) GCD at different current densities from 0.4 A/g to 2A/g of AFO-400 inset show variation in specific capacitance with current densities, (c) plot between log i _{cp} vs log v, (d) plot between i/ v ^{1/2} vs v ^{1/2} at cathodic peak potential and (e, f) corresponds to the Trasatti plot.	82
Figure 3.9: (a) CV of intercalation and surface contribution at 10 mV/s, (b) variation of specific capacity (intercalation vs surface capacitance) at different scan rate, (c) cyclic stability of AFO-400, (d) & (e) represent Nyquist and bode plot of AFO-400 after 1 st and 2000 th cycle.	84

Figure 3.10: (a) Cyclic test of ASC cell at 2 A/g current density during 2000 th cycles, (b) Nyquist plot of ASC cell after 1 st and 2000 th cycles (c) individual CV curves of AFO-400 and AC electrode in three-electrode cell at 50 mV/s scan rate, (d) CV of AFO-400//AC ASC cell recorded within different operational potential window, (e) CV curves of AFO-400//AC recorded as a function of scan rates, and (f) Charge/discharge profile at different current densities.	89
Figure 4.1: XRD pattern of as-prepared K _{0.4} MnO ₂ . xH ₂ O along with the Rietveld refinement study in 2 Θ range of 10-80 $^{\circ}$	96
Figure 4.2: represents the TGA/DTG profile of K _{0.4} MnO ₂ . xH ₂ O under a nitrogen atmosphere.....	98
Figure 4.3: Schematic formation of birnessite-type K _{0.4} MnO ₂ . xH ₂ O.....	98
Figure 4.4: Raman spectra of as-synthesized K _{0.4} MnO ₂ . xH ₂ O.....	99
Figure 4.5: Core level XPS spectrum of (a) Mn 2p, (b) Mn 3s, (c) K 2p, and (d) O 1s. ...	101
Figure 4.6: (a) SEM micrograph, (b), and (c) shows elemental color mapping and EDS spectrum of the selected area of K _{0.4} MnO ₂ . xH ₂ O.....	102
Figure 4.7: (a) the bright-field TEM image of K _{0.4} MnO ₂ . xH ₂ O, (b) & (c) shows the HR-TEM image with inter-planar d-spacing of (001) and (002) plane, and (d) corresponds to the SAED pattern of K _{0.4} MnO ₂ . xH ₂ O.....	103
Figure 4.8: represents the N ₂ adsorption/desorption isotherm of K _{0.4} MnO ₂ . xH ₂ O.	104
Figure 4.9: (a) CV at different scan rates starting from 5 to 100 mV s ⁻¹ , (b) GCD plots at different current densities from 0.5 to 5 A g ⁻¹ , (c) Nyquist plot at open circuit potential in the frequency range 0.1 to 100 kHz, and (d) cyclic performance at 10 A g ⁻¹ current density, inset show GCD curves at various time interval of K _{0.4} MnO ₂ . xH ₂ O electrode.....	106
Figure 4.10: (a) K 2p, and (b) Na 1s core-level XPS spectra of the K _{0.4} MnO ₂ . xH ₂ O electrode at different charge-discharge states. (c) and (d) show Mn 2p _{3/2} core-level XPS spectra at different applied potentials during the cathodic and anodic scans.	107
Figure 4.11: SEM micrograph of K _{0.4} MnO ₂ . xH ₂ O electrode (a) before and (b) after electrochemical cycling.	108
Figure 4.12: (a) log i _{cp} , log i _{ap} vs log ν plot, (b) variation of b with applied potential, (c) plot between i/ $\nu^{1/2}$ vs. $\nu^{1/2}$, (d) CV at 5 mV s ⁻¹ showing intercalation and surface	

contribution separately, (e) intercalation and surface contribution at different scan rate, and (f and g) corresponds to the Trasatti plot of $K_{0.4}MnO_2 \cdot xH_2O$ electrode.	112
Figure 4.13: represents (a) the Rietveld refinement XRD pattern of $AgFeO_2@C$ in 2θ range $10-80^\circ$, (b) Raman spectra of $AgFeO_2@C$, (c) SEM micrograph of $AgFeO_2@C$, and (d) cyclic performance at $10 A g^{-1}$ current density, inset show GCD curves at various time interval of $AgFeO_2@C$ electrode.	114
Figure 4.14: (a) individual CV curves of $K_{0.4}MnO_2 \cdot xH_2O$ and $AgFeO_2@C$ electrodes in a three-electrode cell at $20 mV s^{-1}$ scan rate, (b) CV curves of $AgFeO_2@C // K_{0.4}MnO_2 \cdot xH_2O$ ASC recorded as a function of scan rates, (c) charge/discharge profile at different current densities, (d) Ragone plot of ASC device and inset show glowing of 1.5 V LED, (e) cyclic performance of ASC cell at $5 A g^{-1}$ current density up to 5000 th cycles, and (f) Nyquist plots of ASC cell recorded before 1 st and after 5000 th cycles.	116
Figure 4.15: represents the device fabrication and charge-storage mechanism of the $AgFeO_2@C$ anode and the $K_{0.4}MnO_2 \cdot xH_2O$ cathode in the present ASC system.	119
Figure 5.1: (a) the XRD pattern in 2θ range $10-80^\circ$, (b) the zoom image in 2θ range $32-35^\circ$. (c) Rietveld refinement study collected in 2θ range $10-80^\circ$ and (d) shows % phase fraction analysis of different YSMOs samples.	126
Figure 5.2: Crystal structure showing different pattern of MnO_6 octahedra in (a) YSMO-0, (b) YSMO-50, and (c) YSMO-100.	129
Figure 5.3: (a) the variation of Mn^{3+} and Mn^{4+} in core level XPS of different Sr-doped YSMO samples (YSMO-0, YSMO-50, and YSMO-100), (b) the core level XPS spectra of Sr 3d, Y 3d, Mn 2p, and O 1s of as-synthesized YSMO-50.	130
Figure 5.4: (a) SEM micrograph of as prepared YSMO-50, (b) and (c) elemental colour mapping and EDS spectrum of the selected area.	132
Figure 5.5: (a) bright-field TEM image, (b) HR-TEM with inter-planar d-spacing of (110) plane, (inset: inverse FFT of the selected region with their line profile), and (c) SAED pattern of YSMO-50.	132
Figure 5.6: Nitrogen adsorption/desorption isotherm and corresponding pore size distribution curve (inset) of YSMO-50 powder.	133

Figure 5.7: (a) CV at 20 mV s ⁻¹ scan rate, (b) GCD at 1 A g ⁻¹ current density, and (c) Nyquist plot at open circuit voltage of different electrodes viz. YSMO-0, YSMO-20, YSMO-50, YSMO-70 and YSMO-100.	136
Figure 5.8: (a) CV at different scan rates starting from 2 mV s ⁻¹ to 50 mV s ⁻¹ , (b) GCD at different current densities from 0.5 A g ⁻¹ to 5 A g ⁻¹ , (c) plot between log i _{cp} and log i _{ap} vs log v, (d) plot between i/v ^{1/2} vs v ^{1/2} at peak potential, (e) CV at 20 mV s ⁻¹ showing intercalation and surface contribution separately, (f) intercalation and surface contribution at different scan rate, (g) & (h) corresponds to the Trasatti plot of YSMO-50, (i) & (j) shows cyclic stability test of YSMO-50 and corresponding Nyquist plots taken before 1 st and after 3000 th cycle.	140
Figure 5.9: (a) represents SEM-EDS and (b) shows HR-TEM analysis of YSMO-50 after electrochemical cycling.	143
Figure 5.10: XPS pattern of YSMO-50 at a charging condition of 0.2 V and discharging condition of -0.8 V; (a) Mn 2p XPS spectra, (b) O 1s XPS spectra of the YSMO-50.	144
Figure 5.11: (a) individual CV curves of YSMO-50 and AC electrodes in a three electrode cell set up at 20 mV s ⁻¹ scan rate, (b) CV curves of YSMO-50//AC recorded as a function of scan rates, (c) Charge/discharge profile at different current densities, (d) Cyclic test of ASC cell at 5 A g ⁻¹ current density up to 3000 th cycles, (e) Nyquist plots of ASC cell recorded before 1 st and after 3000 th cycles, and (f) Ragone plot of ASC device	146
Figure 6.1: Shows the (a) XRD, (b) SEM, and (c) high-resolution TEM images of the γ-MnOOH	155
Figure 6.2: (a) XRD pattern, (b) Rietveld refinement study, (c), (d) SEM and (e-h) EDAX analysis with spectrum of LiMnO ₂ -Li ₂ MnO ₃ nanocomposite.	157
Figure 6.3: (a) Bright-field TEM images, (b) SAED pattern, and (c) HR-TEM image of LiMnO ₂ -Li ₂ MnO ₃ nanocomposite (inset show inverse FFT image of area A, B, and C).	158
Figure 6.4: (a) Raman spectra and (b) BET surface area analysis of LiMnO ₂ -Li ₂ MnO ₃ nanocomposite	159
Figure 6.5: (a) The variation of Mn ³⁺ and Mn ⁴⁺ in LiMnO ₂ -Li ₂ MnO ₃ , (b) the core level XPS spectra of Mn 3s, (c) Li 1s, and O 1s in LiMnO ₂ -Li ₂ MnO ₃ nanocomposite.	161
Figure 6.6: Shows the XRD and SEM images of LiMn ₂ O ₄ obtained after heating.....	161

Figure 6.7: (a) LSV at a scan rate of 5 mVs^{-1} in 1 M KOH, (b) ORR activity of different catalysts, (c) overpotentials at a current density of 10 mAcm^{-2} , (d) Tafel plots, (e) LSV comparison $\text{LiMnO}_2\text{-Li}_2\text{MnO}_3$ and RuO_2 , and (f) EIS recorded at 1.54 V vs RHE. 164

Figure 6.8: (a) C_{dl} values, (b) ECSA vs Catalyst, (c) OER attained at 200 mV overpotential vs. ECSA, (d) short CV showing the reduction peak used for active sites determination, (e) The number of active sites vs catalysts, and (f) TOF vs. catalysts. 165

Figure 6.9: Chronoamperometric stability test of $\text{LiMnO}_2\text{-Li}_2\text{MnO}_3$ and inset showing negligible change in the CV profile taken before and after CA experiment 166

Figure 6.10: CV profiles of different synthesized catalysts showing the redox peaks for the oxidation of $\text{Mn}^{\text{III}}/\text{Mn}^{\text{IV}}$ during the OER. 168

Figure 6.11: (a) post-OER SEM images of the $\text{LiMnO}_2\text{-Li}_2\text{MnO}_3$, (b) TEM, (c) SAED pattern of spent $\text{LiMnO}_2\text{-Li}_2\text{MnO}_3$ 169

List of Tables

Table 1.1: Different type of non-renewable and renewable energy source ^[10]	4
Table 1.2: Development of various battery technologies ^[30]	10
Table 3.1: Represents the A ₁ area under the curve of the (105) plane and A ₂ of the (108) plane of various electrodes synthesized at different temperatures.....	73
Table 3.2: Represents the EDS data of AFO-80, fresh AFO-400, and tested AFO-400.....	74
Table 3.3: Represents variation in specific capacitance of AFO-80, AFO-200, AFO-400, and AFO-550 calculated from CV and GCD plots	80
Table 3.4: Represents the rate capability of AFO-400//AC estimated by cyclic voltammetry and charge-discharge experiments.	86
Table 4.1: Structure parameter of K _{0.4} MnO ₂ . xH ₂ O based on Rietveld refinement:	96
Table 4.2: Specific capacitance of K _{0.4} MnO ₂ . xH ₂ O electrode at various scan rates and current densities:	105
Table 4.3: Specific capacitance of AgFeO ₂ @C//K _{0.4} MnO ₂ . xH ₂ O ASC electrode at various scan rates and current densities.....	115
Table 4.4: Comparison of the electrochemical performance of previously reported MnO ₂ -based asymmetric supercapacitor devices with the present work:.....	117
Table 5.1: Structural analysis of different composition of Y _{1-x} Sr _x MnO ₃	128
Table 5.2: Electronic structure of Mn in different composition of Y _{1-x} Sr _x MnO ₃	131
Table 5.3: Compositional analysis of YSMO-50 by the EDS.....	133
Table 5.4: Specific charge storage capacitance of Y _{1-x} Sr _x MnO ₃ electrodes	136
Table 5.5: Parameters of fitting of EIS of different composition of Y _{1-x} Sr _x MnO ₃	137
Table 5.6: Specific capacitance of YSMO-50 at various scan rates and current densities	138
Table 5.7: EIS analysis of YSMO-50 electrode (before and after cycling)	141
Table 5.8: Electronic structure of Mn of YSMO-50 from XPS study at different stage of charge and discharge.....	144
Table 5.9: Specific capacitance of ASC type YSMO-50//AC full cell at various scan rates and current densities	147
Table 5.10: Parameters of fitting of EIS of ASC type YSMO-50//AC full cell electrodes (before and after cycling).....	147

Table 6.1: Structural parameters of $\text{LiMnO}_2\text{-Li}_2\text{MnO}_3$ through Rietveld Refinement.....	156
Table 6.2: Number of active sites, overpotential, TOF, and ECSA normalized current density of different synthesized catalysts.	164
Table 7.1: Showing energy storage capability of different asymmetric supercapacitor devices developed in this thesis.	175

Abbreviations

XRD	X-ray Diffraction
HR-SEM	High-Resolution Scanning Electron Microscope
HR-TEM	High-Resolution Transmission Electron Microscope
TGA	Thermogravimetric analysis
FTIR	Fourier transform Infrared Spectroscopy
XPS	X-ray Photoelectron Spectroscopy
BET	(Brunauer, Emmett, and Teller) specific surface
CV	Cyclic Voltammetry
ASCs	Asymmetric Supercapacitors
Cs	Specific capacitance
A, mA (unit)	Ampere, milliamp
AC	Activated Carbon
C, μC (unit)	Coulomb, microcoulomb
C	Capacitance
C^+/R^+	Cationic species in electrolyte
C^*	Complex differential capacitance
$\text{C}^{+\text{ve}}$	Capacitance of positive electrode
$\text{C}^{-\text{ve}}$	Capacitance of negative electrode
C_{Cell}	Overall cell capacitance
C_{Diff}	Capacitance from diffuse layer
C_{dl}	Capacitance from double layer
C_{g}	Gravimetric capacitance
C_{H}	Capacitance from Helmholtz plane
C_{IH}	Capacitance from inner Helmholtz plane
C_{OH}	Capacitance from outer Helmholtz plan
E°	Standard electrode potential
E_{Total}	Total energy stored in capacitor
EDLC	Electrochemical double layer capacitor

EIS	Electrochemical Impedance Spectroscopy
E_s	Electrochemical supercapacitor
f	Frequency
F	Faraday constant
F	Farad
g	Gram
I	Current
K (unit)	Temperature in Kelvin
k	Boltzmann's constant
M	Molar concentration
Q	Charge
V	Voltage
W (unit)	Watt
Wh (unit)	Watt hour
wt %	Weight percentage
ω	Angular frequency
Z^*	Total impedance
Z'	Real component of impedance
Z''	Imaginary component of impedance
EES	Electrochemical Energy Storage
LSV	Linear Sweep Voltammetry
GCD	Galvanostatic Charge-discharge
CA	Chronoamperometry